Pulsatile Flow Leads to Intimal Flap Motion and Flow Reversal in an *In Vitro* Model of Type B Aortic Dissection

Joav Birjiniuk [ID],[1,9] Lucas H. Timmins,[2] Mark Young,[3] Bradley G. Leshnower,[4] John N. Oshinski,[1,5] David N. Ku,[6,7] and Ravi K. Veeraswamy[8]

[1]Wallace H. Coulter Department of Biomedical Engineering, Georgia Institute of Technology, 315 Ferst Drive, Atlanta, GA 30332-0405, USA; [2]Department of Bioengineering, University of Utah, 36 South Wasatch Drive, Salt Lake City, UT 84112, USA; [3]Cardiac and Vascular Group, Medtronic, Inc., 3576 Unocal Place, Santa Rosa, CA 95403, USA; [4]Division of Cardiothoracic Surgery, Joseph B. Whitehead Department of Surgery, Emory University School of Medicine, 1365 Clifton Road, Atlanta, GA 30322, USA; [5]Department of Radiology and Imaging Sciences, Emory University School of Medicine, 1364 Clifton Road NE Suite D112, Atlanta, GA 30322, USA; [6]George W. Woodruff School of Mechanical Engineering, Georgia Institute of Technology, 315 Ferst Drive, Atlanta, GA 30332-0405, USA; [7]Division of Vascular Surgery, Joseph B. Whitehead Department of Surgery, Emory University School of Medicine, 1365 Clifton Road, Atlanta, GA 30322, USA; [8]Division of Vascular Surgery, Department of Surgery, Medical University of South Carolina, 114 Doughty Street Suite BM 654 MSC 295, Charleston, SC 29425, USA; and [9]Emory University School of Medicine, 1648 Pierce Drive NE, Atlanta, GA 30307, USA

Abstract— Understanding of the hemodynamics of Type B aortic dissection may improve outcomes by informing upon patient selection, device design, and deployment strategies. This project characterized changes to aortic hemodynamics as the result of dissection. We hypothesized that dissection would lead to elevated flow reversal and disrupted pulsatile flow patterns in the aorta that can be detected and quantified by non-invasive magnetic resonance imaging. Flexible, anatomic models of both normal aorta and dissected aorta, with a mobile intimal flap containing entry and exit tears, were perfused with a physiologic pulsatile waveform. Four-dimensional phase contrast magnetic resonance (4D PCMR) imaging was used to measure the hemodynamics. These images were processed to quantify pulsatile fluid velocities, flow rate, and flow reversal. Four-dimensional flow imaging in the dissected aorta revealed pockets of reverse flow and vortices primarily in the false lumen. The dissected aorta exhibited significantly greater flow reversal in the proximal-to-mid dissection as compared to normal (21.1 ± 3.8 vs. $1.98 \pm 0.4\%$, $p < 0.001$). Pulsatility induced unsteady vortices and a pumping motion of the distal intimal flap corresponding to flow reversal. Summed true and false lumen flow rates in dissected models (4.0 ± 2.0 L/min) equaled normal flow rates (3.8 ± 0.1 L/min, $p > 0.05$), validated against external flow measurement. Pulsatile aortic hemodynamics in the presence of an anatomic, elastic dissection differed significantly from those of both steady flow through a dissection and pulsatile flow through a normal aorta. New hemodynamic features including flow reversal, large exit tear vortices, and pumping action of the mobile intimal flap, were observed. False lumen flow reversal would possess a time-averaged velocity close to stagnation, which may induce future thrombosis. Focal vortices may identify the location of tears that could be covered with a stent-graft. Future correlation of hemodynamics with outcomes may indicate which patients require earlier intervention.

Keywords— 4D PCMR, Aortic dissection, Flow model, Hemodynamics, Intimal flap motion.

INTRODUCTION

Thoracic aortic dissection is a potentially fatal condition of the aortic wall affecting between 3 and 4 people per 100,000 yearly.[21,24] Tearing between the layers of the aorta diverts blood flow away from the true lumen into the newly created false lumen, which may result in critical malperfusion of the viscera. Overall in-hospital mortality for patients with Stanford Type B dissection, constrained to the descending aorta, remains at approximately 13%.[39] These patients are initiated on beta-blocker therapy, but may also undergo stent-graft repair of the aorta. In-hospital mortality for both populations remains at 10%, with a nearly 20% 3-year mortality rate for those surviving hospital stay.[27,39] It has been suggested that endovascular intervention in this patient population may promote improved remodeling (i.e., restoration of lumen

Address correspondence to Joav Birjiniuk, Emory University School of Medicine, 1648 Pierce Drive NE, Atlanta, GA 30307, USA. Electronic mail: jbirjin@emory.edu

caliber and flow) of the aorta,[28,29] mitigating long-term sequelae including aneurysm formation. However, it remains unclear why some patients progress to aneurysmal degeneration following endovascular therapy,[27,28] whereas others remain stable with medical therapy alone.

The fluid mechanics of the dissected aorta may be intimately tied to patient outcomes. False lumen thrombosis has emerged as a predictor of patient outcomes, and may explain some of the observed variability in outcomes.[2,13,35–37] While some studies have shown partial thrombosis of the false lumen to portend a worse outcome than a patent false lumen,[2] persistent canalization of the false lumen has been linked to false lumen growth and aneurysmal degeneration.[13,35–37] Though spontaneous and complete thrombosis of the false lumen is a relatively uncommon event,[13] patients exhibiting reversed and recirculating flows within the false lumen may be more likely to develop such complete thrombosis, which is considered a positive prognostic indicator. Current understanding implicates pathologic fluid shear rate as a central mediator of thrombosis.[17,33] Low or stagnant flows (shear rate < 50 s^{-1}) can produce thrombosis *via* the coagulation cascade, whereas extremely high shear flows (> 2000 s^{-1}) lead to platelet aggregation, activation, and thrombosis. Alternatively, low and oscillatory wall shear stress is implicated in atherogenesis[20,26] and endothelial dysfunction,[7,30] ultimately contributing to unfavorable vascular remodeling[5,12,16,30,34] and potential aneurysmal degeneration. Quantification of the wall shear stress may lead to enhanced patient selection for endovascular intervention with better clinical outcomes.

Both computational and experimental approaches have been used to characterize the effects of dissection on aortic hemodynamics. Computational fluid dynamics (CFD) models based on patient-specific aortae have yielded flow fields and shear stresses throughout the aorta at high spatial resolution.[8,9,18] While CFD studies have identified foci of shear extrema, these models have assumed a rigid aortic wall and fixed intimal flap. Lumped parameter models of aortic dissection have shown significantly different hemodynamics between rigid and compliant aortae,[32] with varying modes of flow across dissection tears, indicating the need for including a compliant flap. Recent computational studies have looked to model fluid–structure interactions between the blood and aortic wall,[3] but have yet to include a mobile intimal flap. Some *in vitro* models of dissection possess some compliant features, but have also included either rigid flap[38] or a non-anatomic aortic geometry.[31,38] Full flow fields have not been measured in these physical models,[10] limiting the understanding of salient hemodynamic phenomena, namely flow reversal, secondary flows, and oscillatory shear rate. Thus, full reconstruction of flow fields in models with physiologic flow conditions and mobile intimal flap are considered crucial for study of aortic dissection, particularly in the acute phase.

In order to study the effects of dissection on the hemodynamics of the aorta, we employed a compliant flow phantom of the aorta with a mobile intimal flap[4] subjected to pulsatile flow. By scanning the phantom using 4D phase contrast magnetic resonance imaging (PCMR), full flow fields were acquired throughout the thoracic aorta.[23] This study was aimed at determining changes to normal aortic hemodynamic indices, in particular flow rate and flow reversal, under physiologic flow conditions in the presence of a dissection with a mobile intimal flap. It is hypothesized that under these conditions, the dissected aorta will exhibit increased flow reversal and disruption of pulsatile blood flow as compared to normal.

METHODS

Flow Loop Setup

Silicone models of aortic dissection were fabricated as previously described.[4] Briefly, aortic molds were rapid-prototyped from segmented patient CT images, affording models with realistic, non-aneurysmal dissection geometry. Silicone was cast around the molds in a two-step process in order to form an independent dissection flap and aortic wall. The silicone possessed a stiffness of 1–10 MPa,[6] similar to the stiffness reported for human aorta (0.5–10 MPa).[15,40] Entry and exit tears (one each) were incised circumferentially along the flap on the lateral wall at the flexure of the lesser curvature of the aorta and at a distance four centimeters proximal to the distal lip of the model, respectively (Fig. 1b). Models (one each of normal and dissected) were installed in a flow loop (Fig. 1a) and filled with water to a mean arterial pressure (MAP) of 100 mmHg. Rigid, fiber-reinforced polyvinyl chloride (PVC) tubing was used on the inlet-side of the model to transmit pressure waveforms of 140/80 mmHg with high fidelity (Supplemental Fig. 1). Physiologic flow was initiated at a cardiac index of 4 L/min *via* a custom-made pulsatile positive-displacement pump and measured with a flow meter (Transonic, Ithaca, NY). A multipurpose access catheter (Cook Medical, Bloomington, IA) was advanced antegrade to the proximal ascending aorta and connected to a blood pressure transducer (Harvard Apparatus, Cambridge, MA) to record pressure in the model.
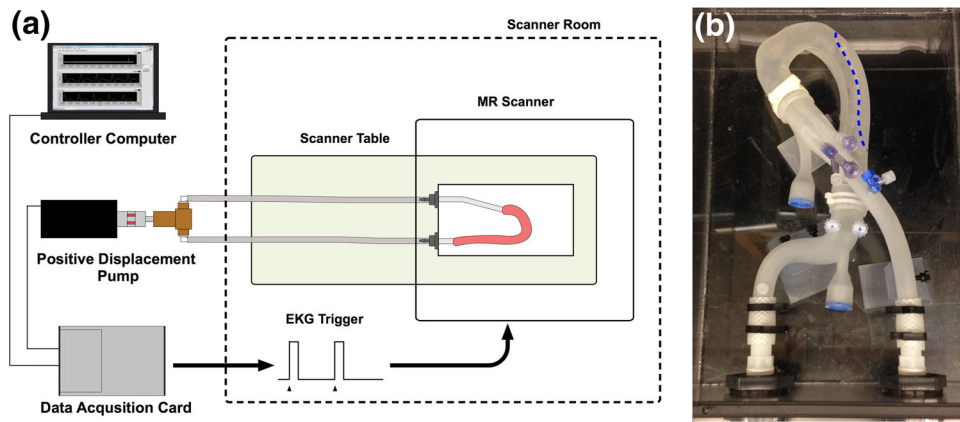
FIGURE 1. Experimental setup for PCMR imaging of aortic dissection model (a). Aortic dissection model (b) with intimal flap outlined (dashed blue).

PCMR Imaging

The magnetic resonance-compatible flow loop was set up in a 3 Tesla Prisma MR scanner (Siemens, Erlangen, Germany), and the model enclosure was filled with water. Tubing was tunneled out to the control room for connection to the pump (Fig. 1). A trigger signal generated by the pump driver was used to provide EKG-gated image acquisition. Four-dimensional PCMR volumes (3 experiments per model) were acquired with a field of view of 250 × 250 mm and slab thickness of 52 mm, covering the entire volume of the model from ascending aorta to the extent of the thoracic aorta, with in-plane resolution of 1.0 mm and slice thickness of 2.0 mm. A velocity encoding value of 80 cm/s in each direction was used to prevent phase-wrapping and optimize the dynamic range of the phases collected. The flip angle was set to 15°, with an echo time of 4.6 ms and repetition time of 59.2 ms. Fifteen phases were acquired over the cardiac cycle resulting in a cardiac period of approximately 888 ms.

Image Processing and Analysis

Aortic wall contours were segmented from magnitude images *via* a region-growing level-set segmentation algorithm using the Medical Imaging Interaction Toolkit (MITK, Heidelberg, Germany). Stereolithography (.stl) files were created from these contours and used to generate point-cloud representations of the aortic lumen. These stereolithography files were also imported into the Vascular Modeling Toolkit (www.vmtk.org) to extract centerlines of the entire aortic lumen. Centerlines, lumen contours, and 4D PCMR volumes were subsequently imported into custom processing software developed in Matlab (Mathworks, Natick, MA).

The segmented aortic contours were used to select data within the aortic lumen (Fig. 2). Phase offset was calculated in each independent phase direction on a slice-by-slice basis and corrected. Vectors tangent to each centerline point were calculated to derive planes normal to the aortic wall. Slices through the phase data were extracted at these planes for calculation of through-plane flow rates. In slices through the dissected portion of the aorta, the dissection flap was manually segmented, allowing for quantification of individual luminal flow rates and areas.

Quantification of Geometric and Hemodynamic Parameters

Geometric parameters were evaluated at 5 slices along the length of the descending aorta. Flap coordinates were parameterized in each slice to generate a spline interpolation in the transverse axis of the intimal flap. Subsequently, a second spline interpolation was performed in the longitudinal direction along the previously interpolated flap points from slice to slice. Flap displacement throughout the cardiac cycle was calculated relative to the initial state (time $t = 0$) as the Euclidean distance between interpolated flap points at 15 equally spaced time points during the cardiac cycle.

Velocity profiles in each lumen were integrated across luminal cross-sections to calculate volumetric flow rate at each cardiac phase. Flow reversal was evaluated by calculating the Reverse Flow Index (RFI), defined as

$$\text{RFI} = 100\% \times \frac{\left| \int_0^T Q_{reverse} dt \right|}{\left| \int_0^T Q_{reverse} dt \right| + \left| \int_0^T Q_{forward} dt \right|}$$
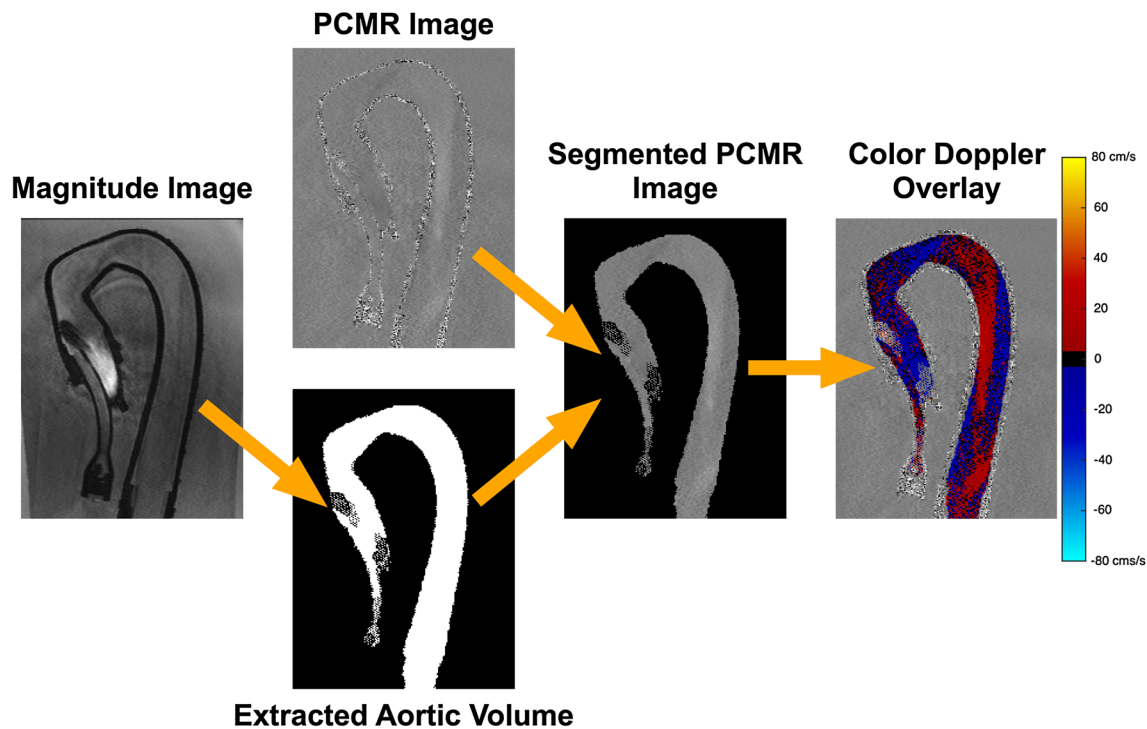
FIGURE 2. Image processing workflow for visualization and hemodynamic calculation. The full volume of the aortic lumen is extracted from the magnitude image, which is then used to segment out velocity data from the aorta alone for processing and visualization.

where Q_{reverse} and Q_{forward} are the summed negative and positive flow rates at a given slice location, respectively, and T is the cardiac period. The RFI quantifies the percentage of blood volume ejected retrograde at a given slice normal to the aortic wall.

Segmented PCMR image stacks for each direction were imported into ParaView (Kitware, Clifton Park, NY) for flow visualization.[1] These stacks were used to define vector components in standard Cartesian directions. Particle paths were calculated across the cardiac cycle and used to visualize flow changes.

Statistical Analysis

Data are reported as mean ± standard deviation. The concordance correlation coefficient (CCC) was calculated to assess agreement[22] between measurements. One-way analysis of variance (ANOVA) tests were performed to compare hemodynamic parameters across normal models and true, false, and total dissected lumina at each individual position in the descending aorta. A p value of 0.05 was set as the level of statistical significance. Pair-wise Tukey–Kramer tests were performed for individual comparisons among groups at each position along the aorta. All statistical analyses were performed in MATLAB (Mathworks, Natick, MA).

RESULTS

Flow Reversal Along Dissection

While true lumen RFI was similar to that of the normal aorta at all planes through the dissection, the false lumen RFI was found to be significantly greater than that of normal in the middle of the dissected segment (Fig. 3). At planes 25 and 50% of the distance between the entry and exit tear, false lumen RFI reached 21.1 ± 3.8 and $16.8 \pm 4.2\%$, respectively, as compared to RFI of 1.98 ± 0.44 and $5.0 \pm 1.6\%$ in the normal aorta ($p < 0.01$ in both cases). False lumen RFI ($1.61 \pm 0.62\%$) was significantly lower than that of the normal aorta ($3.47 \pm 0.50\%$, $p < 0.05$) at the level of the exit tear, while the true lumen had a significantly higher RFI ($5.98 \pm 0.55\%$, $p < 0.01$) than that of the normal at this location, which may be a result of mixing between true and false lumen flows at this location. Reversed flow is observed to occur in both lumina during diastole as the fluid decelerates and the distal false lumen is distended (Fig. 4).

Vortex Formation

A vortex is observed to form in the dissected aorta around the exit tear (Fig. 5; Supplemental Videos 1, 2). During diastole, reversed flows in the distal true lumen
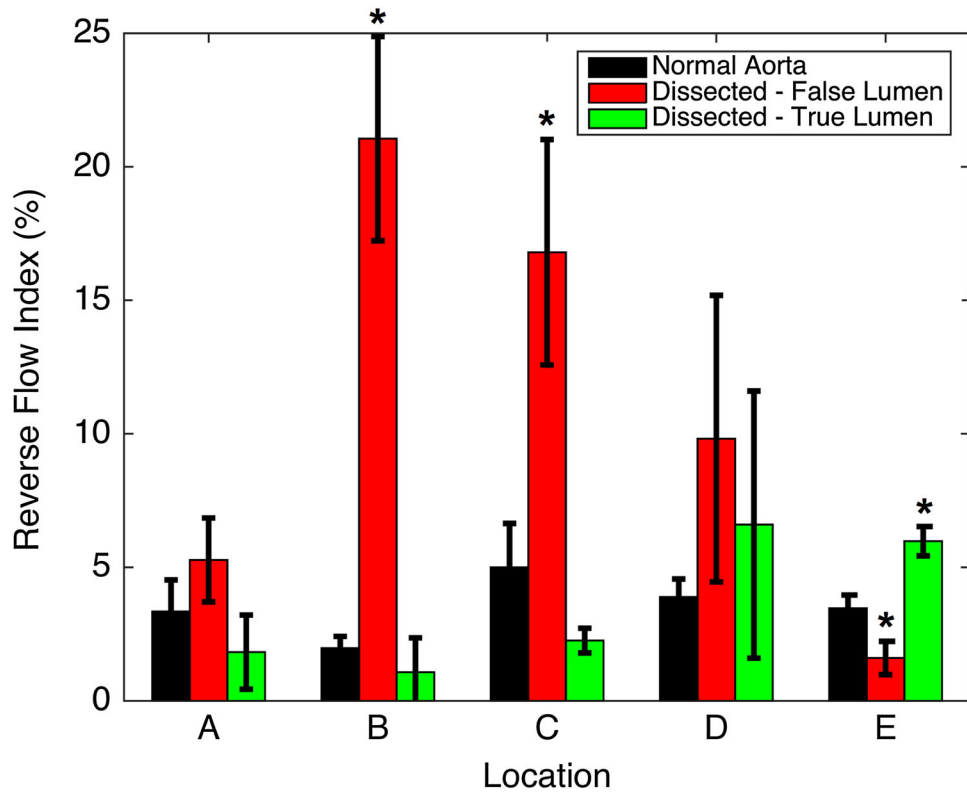
FIGURE 3. Reverse flow index (RFI) calculated in Normal and Dissected aortic lumina at five points along the descending thoracic aorta (asterisk indicates statistical difference from the normal model, $p < 0.05$).
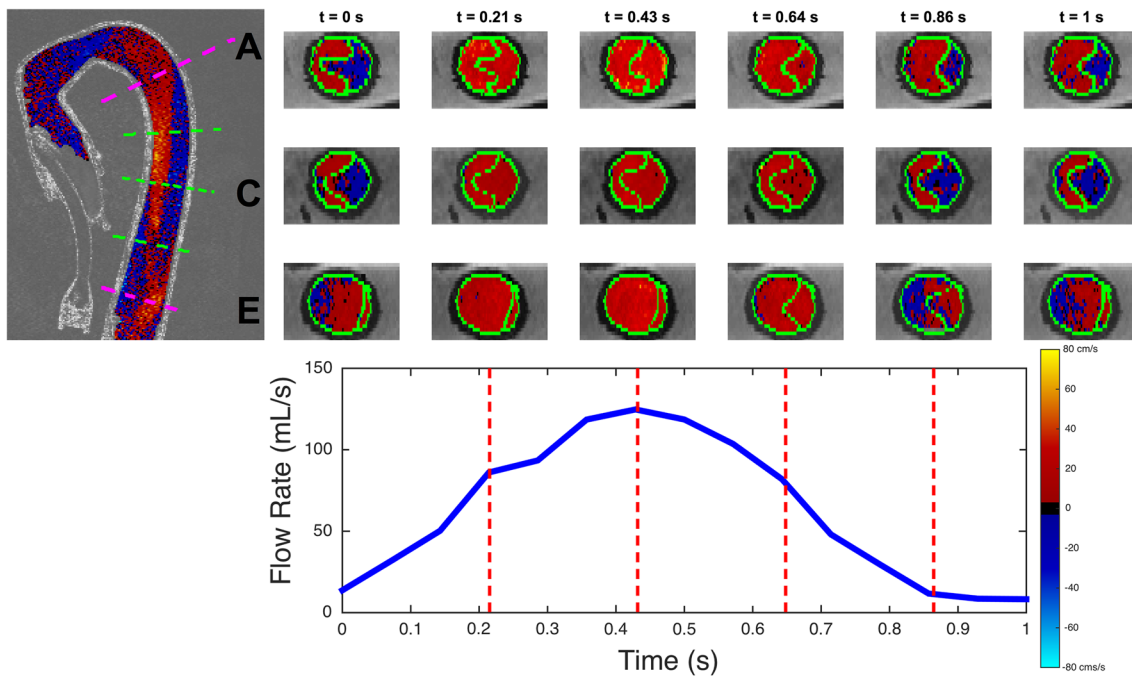

FIGURE 4. Axial slices through the dissection, taken at planes normal to the aortic wall at the level of the entry tear (slice location A), mid-dissection (slice location C), and exit tear (slice location E). Flap motion can be appreciated at all slice locations, but is most accentuated near the exit tear, with flap displacements approaching the aortic radius. Blue indicates retrograde (towards the head) and red antegrade (towards the systemic circulation) flow. Time points of axial slices correspond to positions in the cardiac cycle on the flow waveform below.

are accompanied by forward flow in the false lumen at the exit tear. This may be the result of the mixing of separate streams of varying velocity from each lumen at the exit tear. Shear gradients at such interfaces lead to vortices that evolve with time.

Dynamic Flap Motion

Though the shape of the intimal flap changed along the extent of the dissection, it mainly assumed a sinusoidal cross-sectional profile (Fig. 4). Under pulsatile flow conditions, the intimal flap demonstrated large-scale motion over the course of the cardiac cycle. Greatest displacement of the flap was observed at entry and exit tears (Supplemental Fig. 2, Supplemental Video 2). A maximum displacement of 14.3 ± 0.5 mm, on the order of the aortic radius, was reached near the

exit tear at 0.86 ± 0.07 s of the cardiac cycle, corresponding to mid-diastole. At peak systole (0.43 s), the distal portion of the flap near the exit tear remained collapsed onto the false lumen, achieving maximal true lumen distension (Fig. 4). However, during the deceleration phase and through diastole, the flap moved centrally, leading to a distension of the distal false lumen, up to the exit tear (slice location E), before closing at the end of the cycle. This opening coincided with forward flow in the false lumen near the exit tear, but was delayed in time relative to peak flow more proximally (Fig. 6). Maximal false lumen distension was reached at 0.71 ± 0.07 s, while false lumen flow peaked at 0.38 ± 0.04 s at the entry tear ($p < 0.05$), 0.43 ± 0.07 s at mid-dissection ($p < 0.05$), and 0.52 ± 0.08 s at the level of the exit tear ($p > 0.05$).

Changes to Normal Aortic Velocity Profile

Observation of the normal aortic model in the mid-thoracic descending segment revealed a nearly parabolic velocity profile (Fig. 7) at peak systole. Maximum velocities reached 26.5 ± 2.9 cm/s at 0.45 ± 0.08 s into the cardiac cycle, with minimum velocities of -5.1 ± 1.3 cm/s reached at 0.93 ± 0.07 s. The peak of this profile diminished through the deceleration phase to the end of diastole. A small region of reversed flow was observed along the medial wall of the normal aorta in late diastole. This slight reversal of velocities near the wall is a consequence of the pulsatile aortic flow, as predicted by Womersley.[41] The aortic curvature skews the velocity profile laterally, yielding lesser fluid momentum along the medial wall subject to changes in pressure gradient, leading to marginally reversed flow in this region.

Conversely, the velocity in the dissected aortic model consistently exhibited an eccentric profile. In the mid-thoracic descending aorta, accelerated flows were seen in the compressed true lumen, with peak velocities in the mid-dissection plane of 33.9 ± 4.4 cm/s located at the medial wall occurring at 0.43 s, corresponding to peak systole, above. At this point in time, the well-demarcated false lumen possessed a more parabolic velocity profile, peaking at a velocity of 21.7 ± 1.6 cm/s. However, as the fluid decelerated, the false lumen fluid at mid-dissection level began to reverse, reaching complete luminal reversal, with a minimum velocity of -9.2 ± 1.1 cm/s by the end of diastole (0.90 ± 0.04 s), coinciding with maximal false lumen distension at the exit tear. Collectively, these observations suggest a pumping-like action of flow in the false lumen (i.e., forward flow during systole, reversed flow at end-diastole). Fluid velocities remained positive and antegrade in the mid-thoracic true lumen throughout the cardiac cycle, though a minimum velocity of
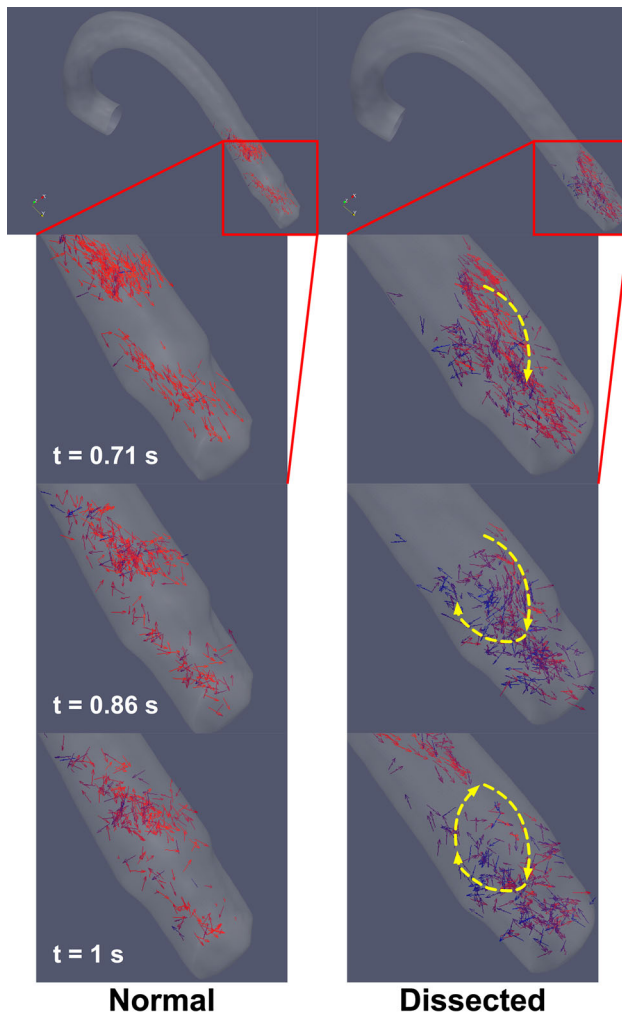

FIGURE 5. Computed flow visualization of MR data documents formation of vortex at exit tear during late diastole in dissected aorta (right). Developing vortical components marked by dotted lines. Absence of large-scale vortices in normal aorta (left).
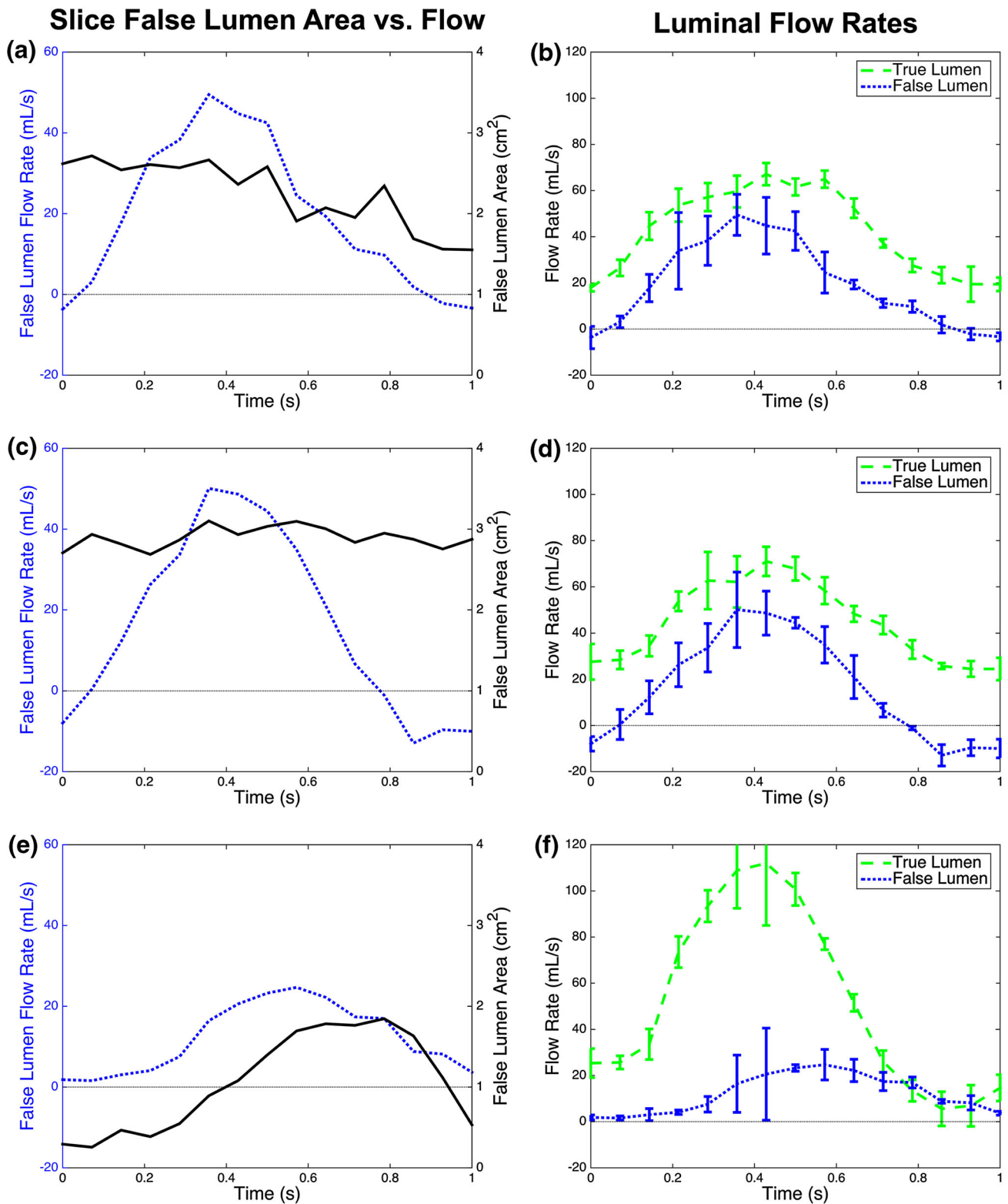
FIGURE 6. False lumen cross-sectional area at exit tear site and corresponding false lumen flow rates (left) and flow division between true and false lumen (right) along the extent of the dissection. Top (a, b), middle (c, d), and bottom (e, f) rows correspond to slice locations A, C, and E, as designated in Fig. 4, respectively. Note forward flow in the false lumen in the proximal and middle dissection as the false lumen is collapsed near the exit tear (area approaches 0) during systole. The false lumen distends during diastole.
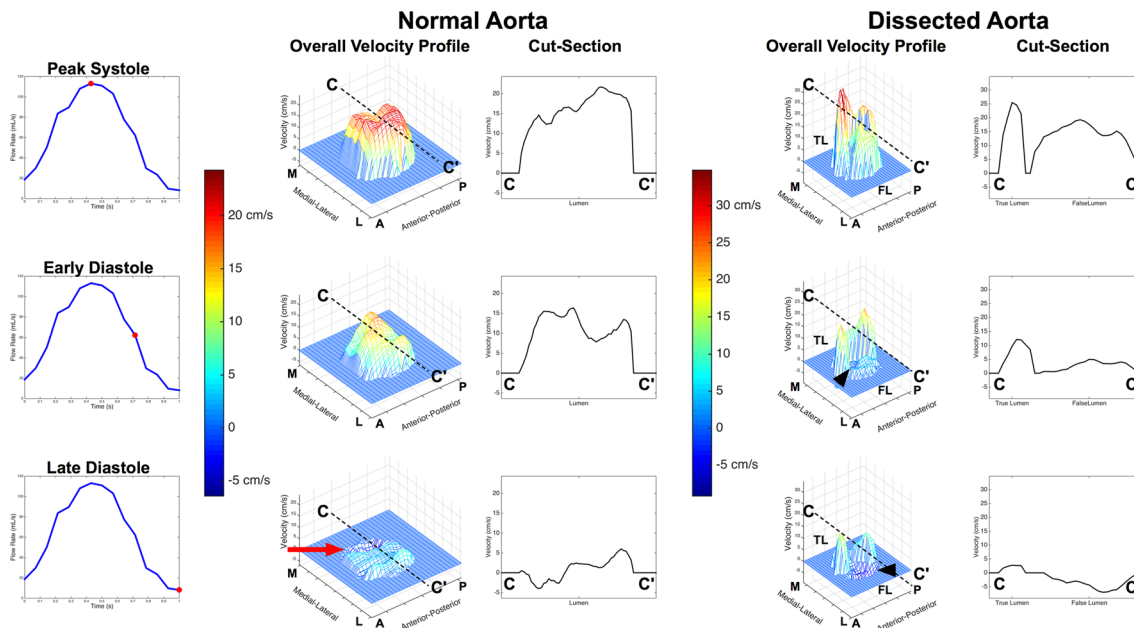
FIGURE 7. Three-dimensional velocity plots in the mid-thoracic descending aorta seen throughout the cardiac cycle. Two-dimensional velocity profiles are taken through the midline of the aortic cross-section along medio-lateral cut plane C–C′. Reversed flow, a consequence of normal pulsatile flow, can be observed along the medial wall of the Normal aorta in late diastole (red arrow). Pathologic reversed flows in the Dissected aorta can be seen originating in the false lumen during the deceleration phase of the cardiac cycle, with fully reversed flow in the false lumen by end diastole (black arrowheads).

-4.3 ± 2.3 cm/s was observed at a point of 0.83 ± 0.04 s within the cardiac period of 1 s.

Flow visualization in both normal and dissected aorta models revealed helical flows developing along the ascending aorta through the aortic arch (Supplemental Fig. 3), as seen physiologically.[19] These complex flows can be appreciated in reconstructed fluid motion (Supplemental Video 1).

Flow Division and Conservation

Overall flow rates were comparable between normal and dissected aortic models (Supplemental Fig. 4). In the descending aorta, flow rates of 4.0 ± 0.2 and 3.8 ± 0.1 L/min were seen in the normal and dissected models, respectively ($p > 0.05$ in comparisons at each slice location). These corresponded to calculated flow rates at model inlet of 4.2 ± 0.3 and 4.1 ± 0.1 L/min ($p = 0.64$) in the normal and dissected models, respectively. However, the flow was divided unequally among true and false lumina, with average flow rates of 2.9 ± 0.3 L/min in the true lumen and 1.0 ± 0.2 L/min in the false ($p < 0.001$ in comparisons at each slice location), corresponding to a mean flow division of 74% to the true lumen with 26% to the false, which was consistent along the length of the dissection ($p > 0.05$ in comparisons between slice locations). While flows peaked in both true and false lumen at

0.44 s in the middle of the dissected segment (Fig. 6), their maximum instantaneous flow rates were significantly different (true lumen: 81 ± 18 mL/s, false lumen: 43 ± 11 mL/s, $p < 0.05$).

Model Reproducibility

Three imaging experiments were performed on the normal and dissected models. The pulsatile pump generated robust, consistent pressure (CCC = 0.94 ± 0.06) and flow (CCC = 0.91 ± 0.02) waveforms throughout experiments. Furthermore, flow rates calculated from PCMR data matched those of the flow meter used in the experimental setup (CCC = 0.96 ± 0.01), validating the flow quantification performed. Finally, calculated flow rates exhibited strong agreement across experiments (CCC = 0.98 ± 0.01, measured at ascending aorta) and all slice locations (Supplemental Fig. 4) along the aorta (CCC = 0.94 ± 0.01).

DISCUSSION

Hemodynamic Alterations in Dissected Aorta

Disruptions to normal pulsatile aortic flow patterns, including flow reversal, luminal pumping, and vortex formation, were discovered in our compliant,

anatomic model of aortic dissection, supporting our initial hypothesis. Significant flow reversal was demonstrated in the proximal false lumen of the dissected aorta when compared to normal controls, as quantified by RFI. Though retrograde flows have been reported in previous clinical studies of dissection,[11,14,25] this phenomenon has not been demonstrated in the laboratory. Reverse flow indices of 20% seen in these regions may account for substantial inefficiency in forward transport of blood through the false lumen.

Pumping action of the false lumen is suspected to account for the observed flow reversal, as undulating motion of the intimal flap coincides with changes in false lumen flow. This action may force fluid retrograde, such that it reverses in the proximal segment by the end of the cycle. Furthermore, closure of the distal false lumen may contribute to the reversed flows observed by substantially increasing resistance in this portion of the dissection. This high resistance may prevent outflow from the proximal false lumen, leading to premature or increased fluid deceleration, and thus reversed flow. These unique fluid dynamic features indicate the critical incorporation of pulsatile flow conditions with mobile intimal flap in this model, along with full reconstruction of the flow field across three spatial dimensions and time, which has not been performed in previous work.

Implications of Altered Hemodynamics

Clinically, the reversed flow burden produces a low mean (time-averaged) wall shear stress that may contribute to natural thrombosis of the false lumen *via* relative fluid stagnation and accumulation of coagulation factors. As a result, patients exhibiting this type of fluid flow in their dissection may have a more favorable outcome due to obliteration of the false lumen with restoration of true lumen flow and caliber over time, which would be expected to decrease the risk of aneurysmal degeneration. The observed flap motion, which is posited to create a pumping mechanism for flow reversal, may be reduced by a stiff or rigid intimal flap. With such stiffening, the false lumen may not achieve occlusive thrombosis once the chronic phase (>30 days) of dissection is reached. Early endovascular intervention may aid in restoring true lumen caliber and promote thrombosis in the false lumen.

These hemodynamic features, however, may in fact promote adverse, pathological vascular remodeling leading to false lumen aneurysm formation. Characterization of the local hemodynamics may ultimately be both a prognostic marker and indication for more aggressive or earlier intervention. Further study of the remodeling of the dissected media due to hemodynamic changes may provide predictions of the natural history for individual patients.

As these luminal streams of different velocity rejoin at the exit tear, a shear, or mixing, layer is formed. Velocity discontinuities at the interface lead to the formation of small, local, vortices. These mixing vortices may induce significant drag and stall, leading to decreased fluid energy and blood transport as a result. Clinically, this may exacerbate endothelial dysfunction promoted by reversed flow and may also contribute to deficient perfusion pressure distally.

Clinical Utility of Functional Flow Imaging

Whereas the workup of dissection has traditionally relied on structural imaging, we suggest the need for functional flow imaging in the assessment of these patients. Both MRI[11,14] and transesophageal echocardiography[25] (TEE) can be used in an EKG-gated fashion to assess pulsatile aortic fluid mechanics. These modalities can be used to quantify flow reversal throughout the dissected aorta, which may prove a useful prognostic indicator. In addition, the visualization of vortical structures with either modality may be used to identify tears in the intimal flap. The location of tears may be important landmarks requiring graft coverage to ensure complete false lumen obliteration. Further study will aid in developing techniques for clinical use.

Model Validity and Utility

As expected, flow rates were conserved in the dissection across true and false lumen, and along the longitudinal extent of the aorta. Though overall flow is maintained, the flow division across the intimal flap indicates significant loss, approximately 25%, to the false lumen with diminished branch vessel perfusion maintained by the true lumen. This perfusion deficiency may itself be an indication for stent-grafting.

We present an experimental model and processing framework for an elastic model of aortic dissection. The custom-built software allows for hemodynamic calculations of flow rates and flow reversal, *via* the RFI, in a reproducible fashion. The rich dynamics of flap motion, pumping, flow reversal, and unsteady vortices have not been identified in previous computational and experimental studies of rigid aortic dissection. In addition, this model allows for validation of flow rates calculated from MRI velocimetry against those measured by flow meter, a feature unavailable in non-invasive human studies employing 4D PCMR.

Limitations

Despite these novel findings, there are some limitations to this work. First, the aortic models used did not contain any branch vessels, in particular, the cephalic vessels originating from the aortic arch. Inclusion of these branches presents a significant technical challenge, as they prohibit the release of the casted silicone from the mold as a single piece, but is an aim of future work. In human physiology, these low-resistance vessels siphon off blood from the aorta to supply the high oxygen demands of the head, neck, and upper extremity, accounting for approximately 15% of the cardiac output. At a physiologic cardiac output of 5 L/min, a corresponding 4.25 L/min would thus be delivered to the descending aorta, similar to the 4 L/min delivered in our model. A skewing of the velocity profile towards the outer curvature of the aortic arch, as seen in the model described, may be strongly accentuated in the presence of the cephalic vessels. Additionally, while the inlet pressure and flow waveforms possessed a slightly extended systolic phase relative to the cardiac period, these conditions were approximately physiologic, and were found to be comparable to those applied in previous work.[10,31,38]

The Emory Biomedical Imaging Technology Center (BITC) limited the fluids allowed for use in the MR scanner to water, with a density of 1000 kg m^{-3} and dynamic viscosity of 0.74 cP, which was used as our working fluid as opposed to blood, which possesses a density of 1060 kg m^{-3} and dynamic viscosity of 3.5 cP. However, the Reynolds number was calculated to be in the laminar range of blood flow in the human aorta, and no transitions to turbulence were observed in the model. The Womersley number calculated for the fluid was in a range similar to that of human aorta, and the relevant effects of pulsatile flow on velocity profiles were observed as predicted.

CONCLUSIONS

In conclusion, we present an *in vitro* methodology and processing workflow to experimentally investigate the hemodynamics of the native and dissected aorta. With this work, we present physiologic flow in a normal aortic model that contrasts with abnormal, reversed flow in a model of a dissected aorta. Vortex identification of tears and general flap motion are measured in the model. These hemodynamic changes may have pathologic consequences in human dissection. Future study of aortic dissection using this experimental setup may improve early, targeted selection of patients for endovascular intervention and may inform upon device design and deployment.

REFERENCES

[1]Ahrens, J., B. Geveci, and C. Law. ParaView: an end-user tool for large data visualization. In: Visualization Handbook, edited by C. D. Hansen, and C. R. Johnson. Cambridge: Academic Press, 2005, pp. 717–731.

[2]Akutsu, K., J. Nejima, K. Kiuchi, K. Sasaki, M. Ochi, K. Tanaka, *et al*. Effects of the patent false lumen on the long-term outcome of type B acute aortic dissection. *Eur. J. Cardiothorac. Surg*. 26:359–366, 2004.

[3]Alimohammadi, M., J. M. Sherwood, M. Karimpour, O. Agu, S. Balabani, and V. Diaz-Zuccarini. Aortic dissection simulation models for clinical support: fluid–structure interaction vs. rigid wall models. *Biomed. Eng. Online* 14:1–16, 2015.

[4]Birjiniuk, J., J. M. Ruddy, E. Iffrig, T. S. Henry, B. G. Leshnower, J. N. Oshinski, *et al*. Development and testing

of a silicone *in vitro* model of descending aortic dissection. *J. Surg. Res.* 198(2):502–507, 2015.

[5]Cecchi, E., C. Giglioli, S. Valente, C. Lazzeri, G. F. Gensini, R. Abbate, *et al.* Role of hemodynamic shear stress in cardiovascular disease. *Atherosclerosis* 214(2):249–256, 2011.

[6]"Characteristic Properties of Silicone Rubber Compounds." Shin-Etsu Co. http://www.silicone.jp/e/catalog/pdf/rubber_e.pdf.

[7]Chatzizisis, Y. S., A. H. Coskun, M. Jonas, E. R. Edelman, C. L. Feldman, and P. H. Stone. Role of endothelial shear stress in the natural history of coronary atherosclerosis and vascular remodeling. *J. Am. Coll. Cardiol.* 49(25):2379–2393, 2007.

[8]Chen, D., M. Müller-Eschner, H. von Tengg-Kobligk, D. Barber, D. Böckler, R. Hose, *et al.* A patient-specific study of type-B aortic dissection: evaluation of true-false lumen blood exchange. *Biomed. Eng. Online* 12:1–16, 2013.

[9]Cheng, Z., N. B. Wood, R. G. J. Gibbs, and X. Y. Xu. Geometric and flow features of type B aortic dissection: initial findings and comparison of medically treated and stented cases. *Ann. Biomed. Eng.* 43(1):177–189, 2015.

[10]Chung, J. W., C. Elkins, T. Sakai, N. Kato, T. Vestring, C. P. Semba, *et al.* True-lumen collapse in aortic dissection: Part I. Evaluation of causative factors in phantoms with pulsatile flow. *Radiology* 214:87–98, 2000.

[11]Clough, R. E., M. Waltham, D. Giese, P. R. Taylor, and T. Schaeffter. A new imaging method for assessment of aortic dissection using four-dimensional phase contrast magnetic resonance imaging. *J. Vasc. Surg.* 55(4):914–923, 2012.

[12]Davies, P. F. Hemodynamic shear stress and the endothelium in cardiovascular pathophysiology. *Nat. Clin. Pract. Cardiovasc. Med.* 6(1):16–26, 2009.

[13]Eggebrecht, H., U. Herold, O. Kuhnt, A. Schmermund, T. Bartel, S. Martini, *et al.* Endovascular stent-graft treatment of aortic dissection: determinants of post-interventional outcome. *Eur. Heart J.* 26(5):489–497, 2005.

[14]François, C. J., M. Markl, M. L. Schiebler, E. Niespodzany, B. R. Landgraf, C. Schlensak, *et al.* Four-dimensional, flow-sensitive magnetic resonance imaging of blood flow patterns in thoracic aortic dissections. *J. Thorac. Cardiovasc. Surg.* 145(5):1359–1366, 2013.

[15]Haskett, D., *et al.* Microstructural and biomechanical alterations of the human aorta as a function of age and location. *Biomech. Model. Mechanobiol.* 9(6):725–736, 2010.

[16]Hwang, J., A. Saha, Y. C. Boo, G. P. Sorescu, J. S. McNally, S. M. Holland, *et al.* Oscillatory shear stress stimulates endothelial production of O_2^- from $p47^{phox}$-dependent NAD(P)H oxidases, leading to monocyte adhesion. *J. Biol. Chem.* 278(47):47291–47298, 2003.

[17]Jackson, J. P. The growing complexity of platelet aggregation. *Blood* 109(12):5087–5095, 2007.

[18]Karmonik, C., S. Partovi, M. Müller-Eschner, J. Bismuth, M. G. Davies, D. J. Shah, *et al.* Longitudinal computational fluid dynamics study of aneurysmal dilatation in a chronic DeBakey type III aortic dissection. *J. Vasc. Surg.* 56(1):260–263.e1, 2012.

[19]Kilner, P. J., G. Z. Yang, R. H. Mohiaddin, D. N. Firmin, and D. B. Longmore. Helical and retrograde secondary flow patterns in the aortic arch studied by three-dimensional magnetic resonance velocity mapping. *Circulation* 88(5):2235–2247, 1993.

[20]Ku, D. N., D. P. Giddens, C. K. Zarins, and S. Glagov. Pulsatile flow and atherosclerosis in the human carotid bifurcation. Positive correlation between plaque location and low oscillating shear stress. *Arterioscler. Thromb. Vasc. Biol.* 5(3):293–302, 1985.

[21]LeMaire, S. A., and L. Russell. Epidemiology of thoracic aortic dissection. *Nat. Rev. Cardiol.* 8(2):103–113, 2011.

[22]Lin, L. I. A concordance correlation coefficient to evaluate reproducibility. *Biometrics* 45(1):255–268, 1989.

[23]Markl, M., A. Frydrychowicz, S. Kozerke, M. Hope, and O. Wieben. 4D Flow MRI. *J. Magn. Reson. Imaging* 36:1015–1036, 2012.

[24]Mészáros, I., J. Mórocz, J. Szlávi, J. Schmidt, L. Tornóci, L. Nagy, *et al.* Epidemiology and clinicopathology of aortic dissection: a population-based longitudinal study over 27 years. *Chest* 117(5):1271–1278, 2000.

[25]Mohr-Kahaly, S., R. Erbel, H. Rennollet, N. Wittlich, M. Drexler, H. Oelert, *et al.* Ambulatory follow-up of aortic dissection by transesophageal two-dimensional and color-coded Doppler echocardiography. *Circulation* 80(1):24–33, 1989.

[26]Moore, J. E., C. Xu, S. Glagov, C. K. Zarins, and D. N. Ku. Fluid wall shear stress measurements in a model of the human abdominal aorta: oscillatory behavior and relationship to atherosclerosis. *Atherosclerosis* 110(2):225–240, 1994.

[27]Nienaber, C. A., and R. E. Clough. Management of acute aortic dissection. *Lancet* 385:800–811, 2015.

[28]Nienaber, C. A., S. Kische, H. Rousseau, H. Eggebrecht, T. C. Rehders, G. Kundt, *et al.* Endovascular repair of type B aortic dissection: long-term results of the randomized investigation of stent-grafts in aortic dissection trial. *Circ. Cardiovasc. Interv.* 6(4):407–416, 2013.

[29]Nienaber, C. A., H. Rousseau, H. Eggebrecht, S. Kische, R. Fattori, T. C. Rehders, *et al.* Randomized comparison of strategies for type B aortic dissection: the Investigation of STEnt grafts in Aortic Dissection (INSTEAD) trial. *Circulation* 120:2519–2528, 2009.

[30]Ranjan, V., Z. Xiao, and S. L. Diamond. Constitutive NOS expression in cultured endothelial cells is elevated by fluid shear stress. *Am. J. Physiol.* 269(2):H550–H555, 1995.

[31]Rudenick, P. A., B. H. Bijnens, D. García-Dorado, and A. Evangelista. An in vitro phantom study on the influence of tear size and configuration on the hemodynamics of the lumina in chronic type B aortic dissections. *J. Vasc. Surg.* 57(2):464–474, 2013.

[32]Rudenick, P. A., B. H. Bijnens, P. Segers, D. García-Dorado, and A. Evangelista. Assessment of wall elasticity variations on intraluminal haemodynamics in descending aortic dissections using a lumped-parameter model. *PLoS ONE* 10(4):e0124011, 2015.

[33]Ruggeri, Z. M. Platelet adhesion under flow. *Microcirculation* 16:58–83, 2009.

[34]Sorescu, G. P., M. Sykes, D. Weiss, M. O. Platt, A. Saha, J. Hwang, *et al.* Bone morphogenic protein 4 produced in endothelial cells by oscillatory shear stress stimulates an inflammatory response. *J. Biol. Chem.* 278(33):31128–31135, 2003.

[35]Sueyoshi, E., I. Sakamoto, K. Hayashi, T. Yamaguchi, and T. Imada. Growth rate of aortic diameter in patients with Type B aortic dissection during the chronic phase. *Circulation* 110(Supplemental II):II256–II261, 2004.

[36]Tanaka, A., M. Sakakibara, H. Ishii, R. Hayashida, Y. Jinno, S. Okumura, *et al.* Influence of the false lumen status on clinical outcomes in patients with acute type B aortic dissection. *J. Vasc. Surg.* 59(2):321–326, 2014.

[37]Tsai, T. T., A. Evangelista, C. A. Nienaber, T. Myrmel, G. Meinhardt, J. V. Cooper, *et al.* Partial thrombosis of the

false lumen in patients with acute type B aortic dissection. *N. Engl. J. Med.* 357(4):349–359, 2007.

[38]Tsai, T. T., M. S. Schlicht, K. Khanafer, J. L. Bull, D. T. Valassis, D. M. Williams, *et al.* Tear size and location impacts false lumen pressure in an ex vivo model of chronic type B aortic dissection. *J. Vasc. Surg.* 47(4):844–851, 2008.

[39]Tsai, T. T., S. Trimarchi, and C. A. Nienaber. Acute aortic dissection: perspectives from the International Registry of Acute Aortic Dissection (IRAD). *Eur. J. Vasc. Endovasc. Surg.* 37(2):149–159, 2009.

[40]Vorp, D. A., *et al.* Wall strength and stiffness of aneurysmal and nonaneurysmal abdominal aorta. *Ann. N. Y. Acad. Sci.* 800:274–276, 1996.

[41]Womersley, J. R. Method for the calculation of velocity, rate of flow and viscous drag in arteries when the pressure gradient is known. *J. Physiol.* 127:553–563, 1955.